Neural Network-based Artifact Detection in Local Field Potentials Recorded from Chronically Implanted Neural Probes

Marcos Fabietti*§, Mufti Mahmud*¶, Ahmad Lotfi*‖, Alberto Averna†**, David Guggenmos‡‡‡, Randolph Nudo‡x and Michela Chiappalone†††
*Dept of Computing & Technology, School of Science and Technology, Nottingham Trent University, Nottingham, UK.
§ORCID: 0000-0003-3093-5985
¶ORCID: 0000-0002-2037-8348 (Corresponding Author)
‖Email: ahmad.lotfi@ntu.ac.uk
†Rehab Technologies, Istituto Italiano di Tecnologia, Genova, Italy.
**ORCID: 0000-0001-9738-1281
††ORCID: 0000-0003-1427-5147
‡Department of Physical Medicine and Rehabilitation, University of Kansas Medical Center, Kansas City, KS USA
‡‡Email: dguggenmos@kumc.edu
xEmail: rnudo@kumc.edu

***Abstract*—The neural recordings known as Local Field Potentials (LFPs) provide important information on how neural circuits operate and relate. Due to the involvement of complex electronic apparatuses in the recording setups, these signals are often significantly contaminated by artifacts generated by a number of internal and external sources. To make the best use of these signals, it is imperative to detect and remove the artifacts from these signals. Hence, this work proposes a pattern recognition neural network based single-channel automatic artifact detection tool. The tool is capable of detecting the artifacts with an 93.2% of overall accuracy and requires an average computing time of 2.57 seconds to analyse LFPs of one minute duration, making it a strong candidate for online deployment without the need for employing high performance computing equipment.**

***Index Terms*—Computational neuroscience, machine learning, physiological signals.**

I. Introduction

The Local Field Potentials (LFPs) are neural signals recorded by micro-electrodes (metal, silicon or glass micropipettes) in deeper layers of the brain, by low pass filtering of the extracellular electrical potential to under 100-300 Hz. The signal obtained encompasses neural processes such as afterpotentials of somato-dendritic spikes, synchronized synaptic potentials and voltage-gated membrane oscillations. They are used to investigate the dynamics and the function of neural circuits under different conditions given their ability to capture different activities within a wide scope of frequencies. Furthermore, they provide stable signal for longer period of time than multi-unit spiking activity, and are therefore useful for long-term chronic experiments and for clinical applications such as brain-machine interfaces [1].

There have been quite some work in developing automated methods in processing and analysing of neuronal signals [2]–[23]. All neural signals are susceptible to noise, labeled as *artifacts* in the domain. They can be originated from internal (physiological) sources or external (non-physiological) ones. Each type has a distinct frequency bands, which are summarized in Table I. Non-physiological artifacts can be of interference kind, such as transmission lines, cellphone signals and light stimulation origin; or instrumental, for instance an electrode's poor contact, popping and lead movement. Physiological artifacts include electrooculogram, electromyogram, electrocardiogram and others. The first category comprehends eye movements, electroretinogram and blinking; while the second one, all muscular activity e.g. chewing, swallowing or talking. The electrocardiogram artifact is produced by the electric activity of the heart, and other sources include skin potentials or respiration [24]. Furthermore, LFP can be contaminated with stimulation artifacts during experiments or spiking activity of local neurons and other distal electrical activity in the brain may be present in the recording.

The importance of the detection and removal of artifacts comes from the undesired effects, from causing a brain-machine interface device to be mistakenly operated, misdiagnosis and disturbance of the study of the brain activity. An example is provided when the use of activity-dependent stimulation paradigm is exploited to modulate cortical state and functional connectivity [25] aimed at improving the behavioral recovery after brain lesion [26]. Since the precise timing for the detection of a spike is crucial to properly pair different population of neurons within this application, an adequate artifact detection algorithm to remove contaminating signals is not neglectable.

There are different approaches to it, such as filtering, manual and automated methods. The first approach consists of using band pass filters on the known frequency bands of an artifact, such as the transmission line artifact being removed by a 50 Hz

978-1-7281-6926-2/20/$31.00 ©2020 IEEE

TABLE I
FREQUENCY BANDS OF ARTIFACTS.

Artifact Types					
Internal				External	
EOG [a]	ECG[b]	EMG[c]	Respiration	Interference	Instrumental
3 -10 Hz	1.2 Hz	0 - 200 Hz	5–10 Hz	50/60 Hz or VHF[d]	VLF[e]

[a] Electrooculogram,[b] Electromyogram,[c] Electrocardiogram ,[d]Very High Frequency and [e]Very Low Frequency.

notch filter. Although, some artifacts have a broad frequency spectrum and can't be easily filtered. The second approach relies on an expert reviewing the neural recording and removing contaminated segments. This requires much expertise in analysis of neural recordings and a considerable amount of time, as well as producing a significant information loss, which is highly undesirable [27]. Alternatively, automated methods could be used which rely on computational algorithms to classify (artifact detection) or recover the original signal (artifact removal), with the aim of preserving the information. While a lot of development has been done over automatic artifact removal, not many of the applications are done in LFP. Neural networks have proven successful on denoising other neural signals, such as electroencephalogram, magnetoencephalography, electrocorticography and spikes. Machine learning has attracted a lot of attention in the recent years. It has been successfully applied to tasks such as biological data mining [28], [29], image analysis [30], financial forecasting [31], anomaly detection [32], disease detection [33], [34], natural language processing [35] and strategic game playing [36]. As for artifact detection and removal, in the literature, we find multi layer perceptron [37]–[45], Convolutional Neural Networks [46]–[48], Recurrent Neural Networks [49], [50], autoencoders [51], [52] and many other architectures [53], [54]. Despite the large amount of architectures and variation available, the most common approach is the Multilayered Perceptron, which has a simple structure and has proven to give good results.

In this study an automatic artifact detection tool based on Neural Networks (NNs) from the unfiltered LFP signal is proposed. Different window sizes are analysed and the model is validated on data recorded in-vivo from freely moving rats. It is shown that NNs can be used to detect artifacts from signal in real time applications without the need for filtering, artifact template subtraction or extracting hand crafted features. The remainder of this paper is organised in 4 sections, in Section II the state of the art present in the literature is described. Section III details the utilized methodology, followed by the obtained results in Section IV. Finally, concluding remarks are made in Section V.

II. STATE OF THE ART

Artifact removal in LFP has been approached with different methodologies in the literature. Qian et al. [55] proposed a technique for the removal of stimulation artifacts during deep brain stimulation, based on stimulus artifact template reconstruction and subtraction. Removing them from LFP signals facilitates the study of how the quantitative dependencies of beta band synchronization varies in the subthalamic nucleus in regards to different stimulation parameters, such as voltage, frequency and pulse width. It was first tested and evaluated in an in-vitro experimental model, then in 26 human participants with Parkinson's disease. The performance was measures as the ratio R, which compares the power spectrum of the recovered useful signal during stimulation with should be the power spectrum of the signal without stimulation, expressed in decibels. Results show that the method improved the signals for all variations of parameters, with the ratio R nearing zero in all situations, indicating that the artifacts were removed. However, this method is limited to offline data processing, and fluctuations of the stimulation waveforms over time as well as inaccuracy of the reconstructed template may cause residual artifacts.

Slow waves (SW) are recurrent fluctuations of LFP that dominate during slow-wave sleep. Bukhtiyarova et al. [56] investigated a new method for identifying SW employing NNs. SWs were acquired from 5 young (2-3 months) male C57Bl/6 mice and manually tagged based on their characteristics, while everything else was tagged as "noise". SW and "noise" exclusive segments were used to train the neural network, which consisted of an input layer, a hidden layer of 20 neurons and two output neurons, one for each class. After 3 to 5 iterations of training, the best performance achieved was 96.1 $\pm$ 1.6% accuracy. As a disadvantage, the tagging process requires an expert to differentiate SWs from "noise" to preselect corresponding templates for each recording electrode.

LFP can be used as an input information to extract motor commands for control of the external devices in brain-machine interfaces. In order to improve the the decoding accuracy of a force signal, Khorasaniet al. [57] applied a weighted common average referencing (CAR) algorithm in combination with Kalman filtering. The algorithm was tested on both simulation and real multi-channel data recorded from 3 freely moving Wistar rats. Before each method, intracortical channels were band-pass filtered remove the DC offset and avoid the aliasing effect, then re-filtered through three spectral sub-bands to obtain LFP features. Finally, those band-pass filtered channels were rectified and low-pass filtered to produce the envelope of different frequency bands and normalized by subtracting the mean values and dividing by standard deviation of each feature. A partial least squares regression model was used to model the relationship between the input feature vector and the output force signal, with the decoding accuracy calculated by measuring the coefficient of determination (R^2) between

978-1-7281-6926-2/20/$31.00 ©2020 IEEE

the actual and predicted force. The experimental study results show that weighted CAR significantly improves decoding performance compared other CAR methods, by achieving R^2 score of 0.39.

Mahmud et al. [58] approached the removal of microstimulation induced stimulus artifacts in LFP via the identification of an artefact's length based on signal derivative and removing it from the recordings through interpolation. This procedure doesn't depend on the shape, duration, and frequency of the artifact unlike other approaches or causes any distortion to the shape of the LFP. It was validated by analyzing recordings from the rat somatosensory cortex, but the authors failed to provide any performance metric, and rely only on on qualitative results as evidence of it.

The methodology proposed in [59] consists of band-pass filtering from 150-400 Hz to detect low frequency artifacts and high-pass filtering at 5 kHz to detect high frequency artifacts. Those band were chosen upon modeling and analysis of the data, where authors concluded that artifacts have different spectrum statistics compared with LFP. From an artifact free, manually labeled, 100 second in-vivo recording a synthetic dataset was built by the addition of different artifacts. The removal procedure for high frequency artifacts is their replacement with a straight line connecting two ends of the artifactual segment. On the other hand, low frequency artifacts, are removed by subtracting the estimated envelope. Test results found that the identification level for artifacts with a magnitude equivalent to neuronal spikes reaches $>80\%$ per cent. Quantitative signal-to-distortion ratio (SDR) simulation revealed that the waveform segments comprising artifacts can have 10-30 dB SDR enhancement.

III. Methods

The recording of the signal, the pre-processing applied to it and the proposed artifact detection model are detailed in the following sub-sections.

A. Signal Acquisition

Five adult, male Long Evans rats weighing 350-400g at 4 months old were used in this experiment. The University of Kansas Medical Center Institutional Animal Care and Use Committee approved the protocols for animal use which adhered to the Guide for the Care and Use of Laboratory Animals (National Research Council (U.S.). Committee for the Update of the Guide for the Care and Use of Laboratory Animals., Institute for Laboratory Animal Research (U.S.), & National Academies Press (U.S.), 2011). The rats were induced with gaseous isoflurane prior to surgery within a sealed vaporizer chamber. Anesthetization followed with injections of ketamine (80-100 mg/kg IP) and xylazine (5-10 mg/kg). Maintenance boluses of ketamine (10-100 mg/kg/h ip or im) were repeatedly injected as needed throughout the procedure. Either Lidocain/Prilocaine cream or bupivacaine were applied to the scalp prior to making a skin incision spanning rostro-caudally between 6 mm rostral to bregma and 5 mm distal to the atlanto-occipital junction. A craniectomy was performed to expose the primary motor (Caudal Forelimb Area: CFA) and premotor (Rostral Forelimb Area: RFA) cortical areas. Electrophysiological procedures were facilitated by removal of the dura and application of sterile silicone oil to the cortex.

A four-shank, sixteen-contact site electrode (A4x4-3mm-100-125-177-CM16LP, NeuroNexus) was chronically implanted into the RFA (premotor cortex) at a maximum depth of 1600 μm. A second four-shank, sixteen-contact electrode (A4x4-3mm-100-125-177-CM16LP, NeuroNexus) was chronically implanted into S1 (forelimb area) and used for stimulation through a single contact. All groups were recorded daily for 21 days. Each animal could move freely inside a self-made plastic cage for the entire duration of each experimental session but was not required to perform any sensorimotor tasks. The daily recording consisted of 80-minute periods of stimulation flanked by a 30-minute period (before stimulation) and a 30-minute period (after stimulation) of no stimulation for a cumulative 2 hours and 20 minutes of recorded data per day. For this research, a subset of the data has been used, which comprises of only the baseline period of recording before stimulation, from 5 different animals for 10 consecutive days.

B. Pre-processing

To obtain LFPs from the acquired data, it was first down-sampled to 1,017.3 Hz and then low-pass filtered (with cutoff frequencies 0-500 Hz) without removing the 60 Hz noise. The LFPs were manually annotated to obtain ground truth about the artifacts. The annotation process consisted of taking LFP chunks composed of 100 datapoints (referred to as bins) and labelling them as 0 (non-artifact) or 1 (artifact), if the total power of the bin exceeds a predefined power threshold which is defined as the mean power of the non-artifacted signal (see Fig. 1). The annotating process didn't aim to identify

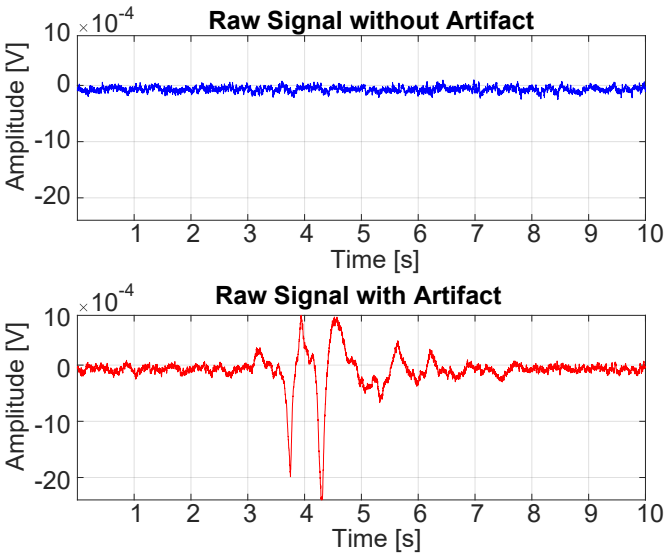

Fig. 1. An example of the raw signals with and without artifact.

978-1-7281-6926-2/20/$31.00 ©2020 IEEE

individual sources of the artifact which can be related to movement, chewing or other different sources.

C. Artifact Detection

To detect artifacts from the preprocessed data, signal chunks with specific window sizes (or bins) were provided to the system. To understand the effect of window size on the artifact detection process, different windows of size 50, 100, 150 and 200 datapoints were constructed and fed to the model. The latter two (i.e., 150 and 200) were created by taking two consecutive bins with the same tag (or label) and expanding the original window (i.e., 100) to avoid mixing of bins containing artifact and non-artifact labels.

To detect the artifacts, a NN-based model was chosen. Inspired by the brain's working principle, the NN-based machine learning algorithms are composed of multiple layers of processing of non-linear information to analyse patterns and classify them. In our approach, the NN uses the application of the hyperbolic tangent ($tanh$) activation function as shown in Eq. 1.

$$f(x) = \frac{2}{1+e^{-2x}} - 1 \tag{1}$$

Here $f(x)$ acts as a step function which squashes a real-valued number to the range [-1, 1] and mimics the behavior of neural activity. The $tanh$ also has its derivative which takes the following form:

$$f'(x) = 1 - f(x)^2 \tag{2}$$

Now, assuming a network with $l = 1, 2, 3, ..., L$ layers, with each layer containing n_l neurons. In our case, n_1 is the dimension of the window size (50, 100, 150 or 200). In broad terms, the network maps from $\mathbb{R}^{n_1}$ to $\mathbb{R}^{n_L}$. The matrix of weights at layer l is expressed as $\boldsymbol{W}^{[l]} \in \mathbb{R}^{n_l \times n_{l-1}}$, and the weight that a neuron j at a layer l applies to the output from a neuron k at a layer $l-1$ as $w_{jk}^{[l]}$. Equivalently, the vector of biases for layer l is expressed as $b^{[l]} \in \mathbb{R}^{n_l}$, and a neuron j at layer l uses the bias $b_j^{[l]}$. Thus, the output of a neuron j at layer l, given an input $x \in \mathbb{R}^{n_1}$ can be expressed as Eq. 3.

$$a^{[l]} = f(W^{[l]} a^{[l-1]} + b_j^{[l]}) \in \mathbb{R}^{n_l}, \text{for } l = 1, 2, 3, ..., L. \tag{3}$$

To train the network and propagate the information, the output of a layer is fed as input to the subsequent unit in the next layer.

Given our dataset with N training bins in $\mathbb{R}^{n_1}$, $\left\{x^{\{i\}}\right\}_{i=1}^{N}$, for which there are target outputs $\left\{y\left(x^{\{i\}}\right)\right\}_{i=1}^{N}$ in $\mathbb{R}^{n_L}$ that correspond to the class label. Consequently, we want to reduce the quadratic cost function shown in Eq. 4.

$$Cost = \frac{1}{N}\sum_{i=1}^{N}\frac{1}{2}\left\|y\left(x^{\{i\}}\right) - a^{[L]}\left(x^{\{i\}}\right)\right\|_2^2, \tag{4}$$

Training the network consists of adjusting the weights and biases in a way that minimizes this cost function in Eq. 4. Once the model is trained, the results of the final output layer are used as the solution for the problem [60].

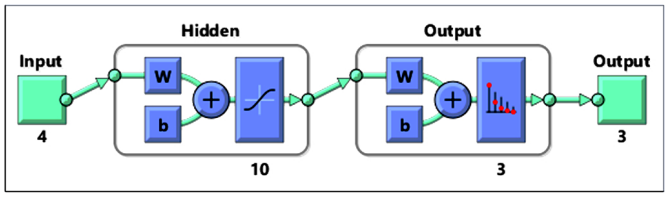

Fig. 2. Basic neural network architecture from the Deep Learning Toolbox from Matlab. It depicts a neural network composed of three layers: an input layer of four neurons, a hidden of ten neurons and an output layer of three neurons.

The NN used in our case was patternet [61] (see Fig. 2 for the basic architecture of the network) from the Deep Learning Toolbox from Matlab [62]. The optimal network architecture was found by training it on smaller sets and adjusting the hidden layer in each iteration. The final model is composed of an input layer of the size of each window, a single hidden layer of 10 neurons and one output neuron.

Given the high imbalance of classes (i.e., artifact vs. non-artifact), the non-artifact data was randomly selected to match the amount of artifact data. Afterwards, it was randomly divided into training (80%), validation (10%) and testing (10%) and used to train the network with the scaled conjugate gradient function *trainscg* [63].

IV. Results and Discussion

The artifact detection task carried out by the NN model was tested on a daily usage grade Acer TravelMate P278-MG laptop consisting of 8 gigabyte of RAM and Intel® Core™ i7- 6500U CPU @ 2.50 GHz processor.

Individual models were constructed for each rodent which were used in predicting the data from the remaining four rodents. The accuracy of these cross-animal models are presented in Fig. 3 A–D, where each row represents the rodent used for constructing the model and each column is the rodent whose data is predicted by the model. In the main diagonal cells are the accuracy of the test set of the neural network training for each model and on the off-diagonal cells, the accuracy of the predictions on the other rodents. It is worth noting that, the results obtained from the prediction task with four different window sizes (50 datapoints as in Fig. 3 A, 100 datapoints as in Fig. 3 B, 150 datapoints as in Fig. 3 C, and 200 datapoints as in Fig. 3 D) show that the highest cross-animal prediction accuracy of the models is obtained at the 150 datapoint window size. Across all window sizes, we can observe that models trained with the data from Rodent 1 achieve the lowest accuracy, while Rodent 5's the highest. This might be attributed to the fact that the data obtained from Rodent 1 has the least number of artifacts (∼110k bins) whereas the data from Rodent 5 has the most number of artifacts (∼445k bins).

Additionally, we trained global models that included randomly selected recordings from all of them, shown in Table II. Due to inter-animal variability, the global model has a reduced accuracy when compared to individual models, nonetheless

978-1-7281-6926-2/20/$31.00 ©2020 IEEE

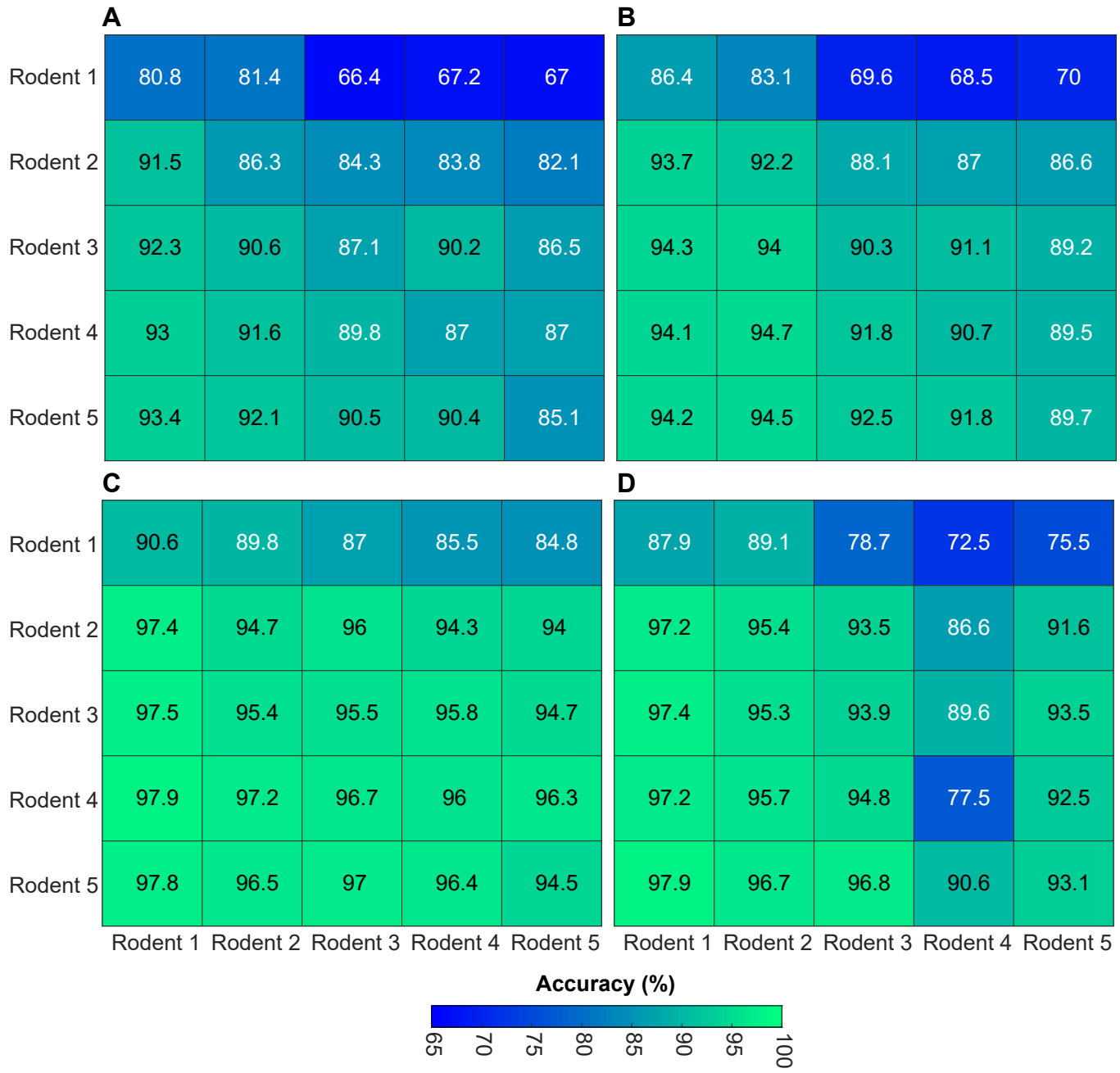

Fig. 3. Individual Model's test accuracy for different window sizes: 50 datapoints in A, 100 datapoints in B, 150 datapoints in C, and 200 datapoints in D. Each row represents the rodent used for constructing the model and each column is the rodent whose data is predicted by the model. In the main diagonal cells are the accuracy of the test set of the neural network training for each model and on the off-diagonal cells, the accuracy of the predictions on the other rodents. The color of each cell represents the achieved Accuracy (%) from the scale depicted at the bottom.

these results suggest that NN can be a practical method for distinguishing artifact signals within and across subjects. The highest accuracy for the global models was achieved as well by the 150 point window, which accounts for 0.147s of recording.

TABLE II
ACCURACY OF THE GLOBAL MODELS BY WINDOW SIZE

Window Size	50	100	150	200
Global Model	85.1 %	89.6%	93.2%	89.2%

The confusion matrix of the test subset for the global 150 point window models can be seen in Fig. 4. In this figure, green colored cells correspond to correctly classified bins and red colored cells to incorrectly classified ones. Both the relative percentage to the overall number of bins and the amount of bins (indicated in bold) are included in the colored

978-1-7281-6926-2/20/$31.00 ©2020 IEEE

cells. The total accuracy is located at the bottom right cell, precision and false discovery rate are displayed in the column on the far right of the plot and the true positive rate and false negative rate are displayed at the bottom row.

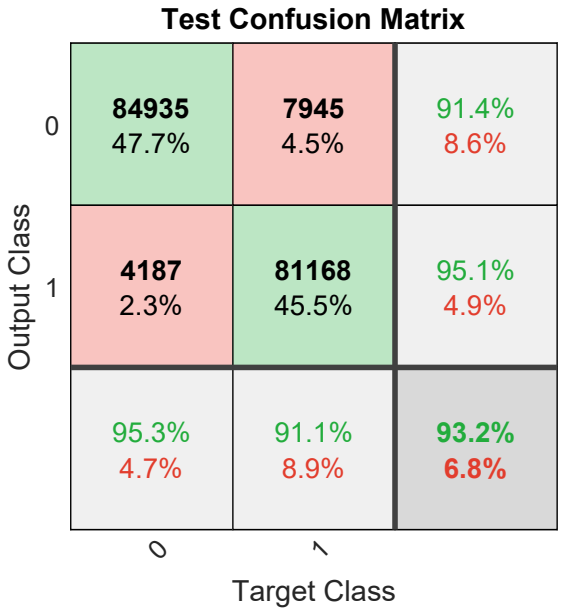

Fig. 4. Global Model's test confusion matrix for the 150 point window model. The rows refer to the class predicted by the NN (Output Class), and the columns refer to the true class (Target Class). Correctly classified bins are located in the diagonal cells (green colored), and incorrectly classified ones in the off-diagonal cells (red colored). In each cell it indicates both the amount of bins (in bold) and relative percentage to the overall number of bins. The precision and false discovery rate are displayed in the column on the far right, while the true positive rate and false negative rate are displayed at the bottom row. Lastly, the total accuracy is indicated at the bottom right cell.

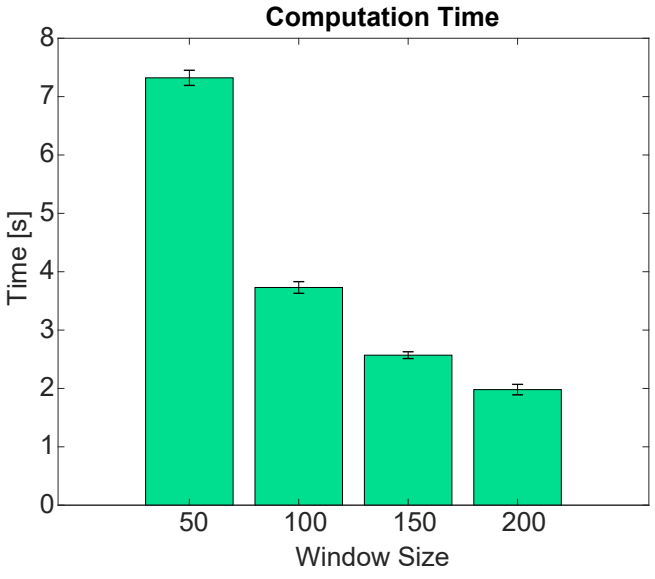

Fig. 5. Computational time by window size, where error bars indicate the standard deviation.

Having achieved a high positive predictability is crucial, as it means that the parts of recording chosen to be removed truly are artifactual. False positives in our models may have originated due to the fact that detection based on the mean threshold of the LFP power is not free of false positives.

Figure 5 displays the average computing time for 1 minute of recording, over 100 iterations for each window size. These results prove to be feasible for online deployment without employing high performance computing. Enlarging the window size reduces the number of batches fed into the network, thus quickening the overall process. Consequently, given the trade-off between the high accuracy and a computing time of 2.57 $\pm$ 0.058 seconds by the 150 window, we select it as the best model.

V. Conclusion

This paper has presented an artifact detection algorithm for in-vivo neural recording. Through the use of NNs, we have achieved an accuracy of 93.2% on a global model. While there is room for improvement, this method doesn't rely on the use of filtering, artifact template subtraction or extracting hand crafted features of the signal. This shows that the neural network has the capacity to extract significant features from the raw signal which allows them to identify artifacts, an improvement over template subtraction, as LFP have complicated shapes. Further pre-processing the signal or a different network architecture, such as recurrent neural network, may boost the results obtained. Nonetheless, these results were obtained on real, un-synthesized data, showing great promise. In the future, we aim to improve the artifact detection and move forward artifact removal via the reconstruction of the original signal. This will allow for us to compare results against the works surveyed in the literature review, as they use other performance metrics.

References

[1] A. Mazzoni, N. K. Logothetis, and S. Panzeri, "Information content of local field potentials," *Principles of neural coding*, pp. 411–429, 2013.

[2] M. Mahmud, S. Girardi, M. Maschietto, M. Rahman, A. Bertoldo, and S. Vassanelli, "Noise Characterization of Electrophysiological Signals Recorded from High Resolution Brain-Chip Interface," in *Proc. ISBB*. RMIT University Press, 2009, p. 84.

[3] M. Mahmud, A. Bertoldo, S. Girardi, M. Maschietto, and S. Vassanelli, "SigMate: A MATLAB-based neuronal signal processing tool," in *Proc. EMBC*. IEEE, 2010, pp. 1352–1355.

[4] M. Mahmud, A. Bertoldo, M. Maschietto, S. Girardi, and S. Vassanelli, "Automatic detection of layer activation order in information processing pathways of rat barrel cortex under mechanical whisker stimulation," in *Proc. EMBC*. IEEE, 2010, pp. 6095–6098.

[5] M. Mahmud, D. Travalin, A. Bertoldo, S. Girardi, M. Maschietto, and S. Vassanelli, "A contour based automatic method to classify local field potentials recorded from rat barrel cortex," in *Proc. CIBEC*. IEEE, 2010, pp. 163–166.

[6] M. Mahmud, S. Girardi, M. Maschietto, A. Bertoldo, and S. Vassanelli, "Processing of neuronal signals recorded by brain-chip interface from surface of the S1 brain cortex," in *Proc. NEBEC*. IEEE, 2010, pp. 1–2.

[7] M. Mahmud, E. Pasqualotto, A. Bertoldo, S. Girardi, M. Maschietto, and S. Vassanelli, "An automated method for detection of layer activation order in information processing pathway of rat barrel cortex under mechanical whisker stimulation," *J. Neurosci. Methods*, vol. 196, no. 1, pp. 141–150, 2011.

978-1-7281-6926-2/20/$31.00 ©2020 IEEE

[8] M. Mahmud, A. Bertoldo, S. Girardi, M. Maschietto, E. Pasqualotto, and S. Vassanelli, "SigMate: A comprehensive software package for extracellular neuronal signal processing and analysis," in *Proc. NER*. IEEE, 2011, pp. 88–91.

[9] M. Mahmud, D. Travalin, A. Bertoldo, S. Girardi, M. Maschietto, and S. Vassanelli, "An automated method for clustering single sweep local field potentials recorded from rat barrel cortex," in *Proc. ISSNIP-BRC*. IEEE, 2011, pp. 1–5.

[10] S. Vassanelli, M. Mahmud, S. Girardi, and M. Maschietto, "On the Way to Large-Scale and High-Resolution Brain-Chip Interfacing," *Cogn. Comput.*, vol. 4, no. 1, pp. 71–81, 2012.

[11] M. Mahmud, M. Maschietto, S. Girardi, and S. Vassanelli, "A Matlab Based Tool for Cortical Layer Activation Order Detection through Latency Calculation in Local Field Potentials Recorded from Rat Barrel Cortex by Brain-Chip Interface," in *Proc. ISSNIP-BRC*. IEEE, 2012, pp. 1–4.

[12] M. Mahmud, D. Travalin, A. Hussain, S. Girardi, M. Maschietto, and S. Vassanelli, "Single LFP Sorting for High-Resolution Brain-Chip Interfacing," in *Proc. BICS*, 2012, pp. 329–337.

[13] M. Mahmud, D. Travalin, and A. Hussain, "Decoding Network Activity from LFPs: A Computational Approach," in *Proc. ICONIP*. Springer, 2012, pp. 584–591.

[14] M. Mahmud, D. Travalin, A. Bertoldo, S. Girardi, M. Maschietto, and S. Vassanelli, "An Automated Classification Method for Single Sweep Local Field Potentials Recorded from Rat Barrel Cortex under Mechanical Whisker Stimulation," *J. Med. Biol. Eng.*, vol. 32, no. 6, pp. 397–404, 2012.

[15] M. Mahmud, R. Pulizzi, E. Vasilaki, and M. Giugliano, "A Web-Based Framework for Semi-Online Parallel Processing of Extracellular Neuronal Signals Re-corded by Microelectrode Arrays," in *Proc. MEAMEETING*. NMI at the University of Tuebingen, Germany, 2014.

[16] M. Mahmud, A. Bertoldo, S. Girardi, M. Maschietto, and S. Vassanelli, "SigMate: A Matlab-based automated tool for extracellular neuronal signal processing and analysis," *J. Neurosci. Methods*, vol. 207, no. 1, pp. 97–112, May 2012.

[17] M. Mahmud, R. Pulizzi, E. Vasilaki, and M. Giugliano, "QSpikeTools: an open source toolbox for parallel batch processing of extracellular neuronal signals recorded by substrate microelectrode arrays," in *Proc. ICEEICT*. IEEE, 2014, pp. 1–6.

[18] C. Cecchetto, M. Mahmud, and S. Vassanelli, "Anesthesia effect on single local field potentials variability in rat barrel cortex: Preliminary results," in *Proc. EMBC*. IEEE, 2015, pp. 4721–4724.

[19] M. Mahmud, R. Pulizzi, E. Vasilaki, and M. Giugliano, "QSpike tools: a generic framework for parallel batch preprocessing of extracellular neuronal signals recorded by substrate microelectrode arrays," *Front. Neuroinform.*, vol. 8, 2014.

[20] M. Mahmud and S. Vassanelli, "Processing and Analysis of Multichannel Extracellular Neuronal Signals: State-of-the-Art and Challenges," *Front. Neurosci.*, vol. 10, 2016.

[21] M. Mahmud, C. Cecchetto, and S. Vassanelli, "An Automated Method for Characterization of Evoked Single-Trial Local Field Potentials Recorded from Rat Barrel Cortex Under Mechanical Whisker Stimulation," *Cogn. Comput.*, vol. 8, no. 5, pp. 935–945, Oct. 2016.

[22] S. Vassanelli and M. Mahmud, "Trends and Challenges in Neuroengineering: Toward "Intelligent" Neuroprostheses through Brain-"Brain Inspired Systems" Communication," *Front. Neurosci.*, vol. 10, 2016.

[23] M. Mahmud and S. Vassanelli, *Open-Source Tools for Processing and Analysis of In Vitro Extracellular Neuronal Signals*. Cham: Springer International Publishing, 2019, pp. 233–250.

[24] A. Tandle and N. Jog, "Classification of artefacts in eeg signal recordings and overview of removing techniques," *International Journal of Computer Applications*, vol. 975, p. 8887, 2015.

[25] A. Averna, V. Pasquale, M. Murphy, M. P. Rogantin, G. Van Acker, R. Nudo, M. Chiappalone, and D. Guggenmos, "Differential effects of open-and closed-loop intracortical microstimulation on firing patterns of neurons in distant cortical areas," *bioRxiv*, p. 534032, 2019.

[26] D. J. Guggenmos, M. Azin, S. Barbay, J. D. Mahnken, C. Dunham, P. Mohseni, and R. J. Nudo, "Restoration of function after brain damage using a neural prosthesis," *Proceedings of the National Academy of Sciences*, vol. 110, no. 52, pp. 21 177–21 182, 2013.

[27] J. A. Urigüen and B. Garcia-Zapirain, "Eeg artifact removal—state-of-the-art and guidelines," *Journal of neural engineering*, vol. 12, no. 3, p. 031001, 2015.

[28] M. Mahmud, M. S. Kaiser, A. Hussain, and S. Vassanelli, "Applications of deep learning and reinforcement learning to biological data," *IEEE transactions on neural networks and learning systems*, vol. 29, no. 6, pp. 2063–2079, 2018.

[29] M. Mahmud, M. S. Kaiser, T. M. McGinnity, and A. Hussain, "Deep Learning in Mining Biological Data," *arXiv*, vol. abs/2003.00108, pp. 1–36, 2020.

[30] H. M. Ali, M. S. Kaiser, and M. Mahmud, "Application of convolutional neural network in segmenting brain regions from mri data," in *International Conference on Brain Informatics*. Springer, 2019, pp. 136–146.

[31] O. Orojo, J. Tepper, T. M. McGinnity, and M. Mahmud, "A Multi-recurrent Network for Crude Oil Price Prediction," in *Proceedings of the 2019 IEEE Symposium Series on Computational Intelligence (SSCI)*, 2019, pp. 2953–2958.

[32] S. W. Yahaya, A. Lotfi, and M. Mahmud, "A consensus novelty detection ensemble approach for anomaly detection in activities of daily living," *Applied Soft Computing*, vol. 83, p. 105613, 2019.

[33] M. B. T. Noor, N. Z. Zenia, M. S. Kaiser, M. Mahmud, and S. Al Mamun, "Detecting neurodegenerative disease from mri: A brief review on a deep learning perspective," in *International Conference on Brain Informatics*. Springer, 2019, pp. 115–125.

[34] Y. Miah, C. N. E. Prima, S. J. Seema, M. Mahmud, and M. S. Kaiser, "Performance comparison of machine learning techniques in identifying dementia from open access clinical datasets," in *Proc. ICACIn*. Springer, Singapore, 2020, pp. 69–78.

[35] G. Rabby, S. Azad, M. Mahmud, K. Z. Zamli, and M. M. Rahman, "Teket: a tree-based unsupervised keyphrase extraction technique," *Cognitive Computation*, 2020, doi: 10.1007/s12559-019-09706-3, [epub ahead of print].

[36] D. Silver, A. Huang, C. J. Maddison, A. Guez, L. Sifre, G. Van Den Driessche, J. Schrittwieser, I. Antonoglou, V. Panneershelvam, M. Lanctot *et al.*, "Mastering the game of go with deep neural networks and tree search," *nature*, vol. 529, no. 7587, p. 484, 2016.

[37] D. Issar, R. C. Williamson, S. B. Khanna, and M. A. Smith, "A neural network for online spike classification that improves decoding accuracy," *BioRxiv*, p. 722934, 2019.

[38] J. Wu, E. Ifeachor, E. Allen, S. Wimalaratna, and N. Hudson, "Intelligent artefact identification in electroencephalography signal processing," *IEE Proceedings-Science, Measurement and Technology*, vol. 144, no. 5, pp. 193–201, 1997.

[39] M. Paulraj, S. B. Yaccob, and C. Yogesh, "Fractal feature based detection of muscular and ocular artifacts in eeg signals," in *2014 IEEE Conference on Biomedical Engineering and Sciences (IECBES)*. IEEE, 2014, pp. 916–921.

[40] T. Radüntz, J. Scouten, O. Hochmuth, and B. Meffert, "Automated eeg artifact elimination by applying machine learning algorithms to ica-based features," *Journal of neural engineering*, vol. 14, no. 4, p. 046004, 2017.

[41] A. A. Gharbali, J. M. Fonseca, S. Najdi, and T. Y. Rezaii, "Automatic eog and emg artifact removal method for sleep stage classification," in *Doctoral Conference on Computing, Electrical and Industrial Systems*. Springer, 2016, pp. 142–150.

[42] C. Guerrero-Mosquera and A. N. Vazquez, "Automatic removal of ocular artifacts from eeg data using adaptive filtering and independent component analysis," in *2009 17th European Signal Processing Conference*. IEEE, 2009, pp. 2317–2321.

[43] M. A. Sovierzoski, L. Schwarz, and F. M. de Azevedo, "Binary neural classifier of raw eeg data to separate spike and sharp wave of the eye blink artifact," in *2009 Fifth International Conference on Natural Computation*, vol. 2. IEEE, 2009, pp. 126–130.

[44] R. Ksiezyk, K. Blinowska, P. Durka, W. Szelenberger, and W. Androsiuk, "Neural networks with wavelet preprocessing in eeg artifact recognition," in *Abstract of Medicon Conference*, 1998, pp. 23–95.

[45] G. Kang, S.-H. Jin, D. K. Kim, and S. W. Kang, "T59. eeg artifacts removal using machine learning algorithms and independent component analysis," *Clinical Neurophysiology*, vol. 129, p. e24, 2018.

[46] A. Hasasneh, N. Kampel, P. Sripad, N. J. Shah, and J. Dammers, "Deep learning approach for automatic classification of ocular and cardiac artifacts in meg data," *Journal of Engineering*, vol. 2018, 2018.

[47] P. Garg, E. Davenport, G. Murugesan, B. Wagner, C. Whitlow, J. Maldjian, and A. Montillo, "Using convolutional neural networks to automatically detect eye-blink artifacts in magnetoencephalography without resorting to electrooculography," in *International Conference on Medical*

978-1-7281-6926-2/20/$31.00 ©2020 IEEE

Image Computing and Computer-Assisted Intervention. Springer, 2017, pp. 374–381.

[48] M. Saif-ur Rehman, R. Lienkämper, Y. Parpaley, J. Wellmer, C. Liu, B. Lee, S. Kellis, R. Andersen, I. Iossifidis, T. Glasmachers *et al.*, "Universal spike classifier," *arXiv preprint arXiv:1811.02923*, 2018.

[49] A. Erfanian and B. Mahmoudi, "Real-time ocular artifact suppression using recurrent neural network for electro-encephalogram based brain-computer interface," *Medical and Biological Engineering and Computing*, vol. 43, no. 2, pp. 296–305, 2005.

[50] S. Selvan and R. Srinivasan, "Recurrent neural network based efficient adaptive filtering technique for the removal of ocular artefacts from eeg," *IETE Technical Review*, vol. 17, no. 1-2, pp. 73–78, 2000.

[51] B. Yang, K. Duan, and T. Zhang, "Removal of eog artifacts from eeg using a cascade of sparse autoencoder and recursive least squares adaptive filter," *Neurocomputing*, vol. 214, pp. 1053–1060, 2016.

[52] N. M. N. Leite, E. T. Pereira, E. C. Gurjao, and L. R. Veloso, "Deep convolutional autoencoder for eeg noise filtering," in *2018 IEEE International Conference on Bioinformatics and Biomedicine (BIBM)*. IEEE, 2018, pp. 2605–2612.

[53] F. Rong and J. L. Contreras-Vidal, "Magnetoencephalographic artifact identification and automatic removal based on independent component analysis and categorization approaches," *Journal of neuroscience methods*, vol. 157, no. 2, pp. 337–354, 2006.

[54] L. Routray, P. Biswal, and S. R. Pattanaik, "Ecg artifact removal of eeg signal using adaptive neural network," in *2018 IEEE 13th International Conference on Industrial and Information Systems (ICIIS)*. IEEE, 2018, pp. 103–106.

[55] X. Qian, Y. Chen, Y. Feng, B. Ma, H. Hao, and L. Li, "A method for removal of deep brain stimulation artifact from local field potentials," *IEEE Transactions on Neural Systems and Rehabilitation Engineering*, vol. 25, no. 12, pp. 2217–2226, 2016.

[56] O. Bukhtiyarova, S. Soltani, S. Chauvette, and I. Timofeev, "Supervised semi-automatic detection of slow waves in non-anaesthetized mice with the use of neural network approach," 2016.

[57] A. Khorasani, V. Shalchyan, and M. R. Daliri, "Adaptive artifact removal from intracortical channels for accurate decoding of force signal in freely moving rats," *Frontiers in Neuroscience*, vol. 13, p. 350, 2019.

[58] M. Mahmud, S. Girardi, M. Maschietto, and S. Vassanelli, "An automated method to remove artifacts induced by microstimulation in local field potentials recorded from rat somatosensory cortex," in *2012 ISSNIP Biosignals and Biorobotics Conference: Biosignals and Robotics for Better and Safer Living (BRC)*. IEEE, 2012, pp. 1–4.

[59] M. K. Islam, N. A. Tuan, Y. Zhou, and Z. Yang, "Analysis and processing of in-vivo neural signal for artifact detection and removal," in *2012 5th International Conference on BioMedical Engineering and Informatics*. IEEE, 2012, pp. 437–442.

[60] C. F. Higham and D. J. Higham, "Deep learning: An introduction for applied mathematicians," *SIAM Review*, vol. 61, no. 4, pp. 860–891, 2019.

[61] V. Arulmozhi, "Classification task by using matlab neural network tool box–a beginner's view," *International Journal of Wisdom Based Computing*, vol. 1, no. 2, pp. 59–60, 2011.

[62] MATLAB. Deep Learning Toolbox R2019a. The MathWorks Inc., Natick, Massachusetts, United States, 2017.

[63] M. F. Møller,"A Scaled Conjugate Gradient Algorithm for Fast Supervised Learning," *DAIMI Report Series*, vol. 19, no. 339, Jan. 1990.

978-1-7281-6926-2/20/$31.00 ©2020 IEEE